

CO SPECTRAL LINE ENERGY DISTRIBUTIONS IN GALACTIC SOURCES: EMPIRICAL INTERPRETATION OF EXTRAGALACTIC OBSERVATIONS ^a

NICK INDRIOLO¹ & E. A. BERGIN

Department of Astronomy, University of Michigan, 1085 S. University Ave., Ann Arbor, MI 48109, USA

J. R. GOICOECHEA & J. CERNICHARO

Grupo de Astrofísica Molecular, Instituto de Ciencia de Materiales de Madrid (CSIC). E-28049. Madrid, Spain

M. GERIN & A. GUSDORF

LERMA, Observatoire de Paris, PSL Research University, CNRS, Sorbonne Universités, UPMC Univ. Paris 06, École normale supérieure, F-75005, Paris, France

D. C. LIS²

LERMA, Observatoire de Paris, PSL Research University, CNRS, Sorbonne Universités, UPMC Univ. Paris 06, F-75014, Paris, France

P. SCHILKE

I. Physikalisches Institut der Universität zu Köln, Zùlpicher Str. 77, 50937 Köln, Germany

¹Current address: Space Telescope Science Institute, Baltimore, MD 21218, USA; nindriolo@stsci.edu

²California Institute of Technology, Cahill Center for Astronomy and Astrophysics 301-17, Pasadena, CA 91125, USA

ABSTRACT

The relative populations in rotational transitions of CO can be useful for inferring gas conditions and excitation mechanisms at work in the interstellar medium. We present CO emission lines from rotational transitions observed with *Herschel*/HIFI in the star-forming cores Orion S, Orion KL, Sgr B2(M), and W49N. Integrated line fluxes from these observations are combined with those from *Herschel*/PACS observations of the same sources to construct CO spectral line energy distributions (SLEDs) from $5 \leq J_u \leq 48$. These CO SLEDs are compared to those reported in other galaxies, with the intention of empirically determining which mechanisms dominate excitation in such systems. We find that CO SLEDs in Galactic star-forming cores cannot be used to reproduce those observed in other galaxies, although the discrepancies arise primarily as a result of beam filling factors. The much larger regions sampled by the *Herschel* beams at distances of several Mpc contain significant amounts of cooler gas which dominate the extragalactic CO SLEDs, in contrast to observations of Galactic star-forming regions which are focused specifically on cores containing primarily hot molecular gas.

1. INTRODUCTION

The *Herschel* Space Observatory (Pilbratt et al. 2010) enabled the first surveys of rotational transitions of CO with $4 \leq J_u \leq 50$ in emission throughout a wide sample of galaxies. These CO emission lines can be used to place constraints on the physical conditions (e.g., density, temperature, radiation field) within the emitting gas as the relative populations in the various rotational states are controlled by collisional and radiative (de)-excitation. The shape of the CO Spectral Line Energy Distribution (SLED)—flux in each emission line as a function of upper state energy—

^a *Herschel* is an ESA space observatory with science instruments provided by European-led Principal Investigator consortia and with important participation from NASA.

provides information about the gas conditions, and potentially the agent (e.g., shocks, X-rays, UV photons, cosmic rays) primarily responsible for heating the gas. Multiple observing programs targeted CO emission lines in the central regions of different types of galaxies—e.g., Ultra-Luminous InfraRed Galaxies (ULIRGs), Seyfert galaxies, starburst galaxies—for the purpose of determining which of the aforementioned mechanisms dominate the gas heating in each case. However, in most galaxies the observed CO SLEDs can be fit with a variety of models, such that it is difficult to conclude whether shocks, PDRs (photon dominated regions), or XDRs (X-ray dominated regions), are driving the CO excitation (e.g., [Hailey-Dunsheath et al. 2012](#); [Kamenetzky et al. 2014](#); [Mashian et al. 2015](#); [Rosenberg et al. 2015](#)). While kinematic information would provide a clue to this puzzle, both the SPIRE (Spectral and Photometric Imaging Receiver; [Griffin et al. 2010](#)) and PACS (Photoconductor Array Camera and Spectrometer; [Poglitsch et al. 2010](#)) instruments used for these extragalactic observations are incapable of spectrally resolving the CO emission lines.

Herschel observations of CO emission lines have also been reported for a variety of regions within our Galaxy, including the well-studied objects Sgr B2 ([Etxaluze et al. 2013](#)), Sgr A ([Goicoechea et al. 2013](#)), and Orion KL ([Goicoechea et al. 2015](#)). In some Galactic sources, however, in addition to the low spectral resolution PACS data we also have *Herschel* HIFI (Heterodyne Instrument for the Far Infrared; [de Graauw et al. 2010](#)) observations of $J_u \leq 16$ transitions of CO that are spectrally resolved. By studying the velocity profiles of these CO emission lines in Galactic sources we can better constrain the excitation mechanisms involved in producing different CO SLED shapes.

Galactic regions that we consider herein include the Orion Bar, Orion South, Orion KL, Sgr B2(M), and W49N. The Orion Bar is a prototypical strongly illuminated PDR, and is located in the Orion star forming region at a distance of 414 pc ([Menten et al. 2007](#)). It has the distinction of being nearly “edge-on”, such that the atomic and molecular emission from different stratified layers can be studied (e.g., [van der Wiel et al. 2009](#); [Nagy et al. 2013](#)). Orion S is an embedded star-forming region that contains multiple outflows ([Ziurys et al. 1990](#); [Schmid-Burgk et al. 1990](#); [Zapata et al. 2005, 2006](#)), shocked gas ([Henney et al. 2007](#); [Rivilla et al. 2013](#)), and a PDR illuminated by the Trapezium stars ([Peng et al. 2012](#)). In Section 4.2 we show that the CO emission profiles in Orion S can be decomposed into these three components. Orion KL is a luminous, high-mass star forming region comprised of multiple spatial and kinematic components. It harbors warm gas clumps, multiple suspected protostars, quiescent gas, and shocked gas resulting from explosive outflows ([Blake et al. 1987](#); [Zapata et al. 2009, 2011](#); [Nissen et al. 2012](#); [Crockett et al. 2014](#)). Sgr B2(M) is a compact, massive, star-forming core within the central molecular zone of our Galaxy, and its surrounding envelope is an X-ray reflection nebula ([Murakami et al. 2000](#)). W49N is one of the most luminous and massive star-forming regions within our Galaxy ([Galván-Madrid et al. 2013](#), and references therein), harboring multiple star clusters and tens of O-type stars ([Alves & Homeier 2003](#); [Wu et al. 2016](#)). It is frequently referred to as a starburst region in comparison to the eponymous class of galaxies. Through analysis of the CO SLEDs in these different well-studied, well-characterized Galactic regions, we aim to empirically interpret extragalactic CO SLEDs.

2. OBSERVATIONS

The HEXOS (*Herschel* observations of EXtra-Ordinary Sources; KPGT_ebergin_1; [Bergin et al. 2010](#)) key program includes scans over the full spectral range of HIFI (480–1906 GHz, with gaps from 1280–1430 GHz and 1540–1570 GHz) toward Orion KL $[(\alpha, \delta) = (05^{\text{h}}35^{\text{m}}14^{\text{s}}.3, -05^{\circ}22'33.7'')]$, Orion South $[(\alpha, \delta) = (05^{\text{h}}35^{\text{m}}13^{\text{s}}.4, -05^{\circ}24'08.1'')]$, the Orion Bar $[(\alpha, \delta) = (05^{\text{h}}35^{\text{m}}20^{\text{s}}.6, -05^{\circ}25'14.0'')]$, Sgr B2(M) $[(\alpha, \delta) = (17^{\text{h}}47^{\text{m}}20^{\text{s}}.35, -28^{\circ}23'03.0'')]$, and Sgr B2(N) $[(\alpha, \delta) = (17^{\text{h}}47^{\text{m}}19^{\text{s}}.88, -28^{\circ}22'18.4'')]$. Targets were observed in dual beam switch (DBS) spectral scan mode with reference positions offset by $3'$, and the wide band spectrometer (WBS) was employed to provide 1.1 MHz resolution. In all sources, the HIFI spectra cover rotational transitions of $^{12}\text{C}^{16}\text{O}$ (hereafter referred to simply as CO) out of the $5 \leq J_u \leq 16$ levels.¹ Toward Orion KL, however, the HIFI beam does not encompass the entire emitting region for $J_u \geq 13$, so for these transitions there are separate pointings toward the hot core $[(\alpha, \delta) = (05:35:14.5, -05:22:30.9)]$ and compact ridge $[(\alpha, \delta) = (05:35:14.1, -05:22:36.5)]$ components ([Crockett et al. 2014](#)). Individual analyses of the full spectra have been reported for Orion KL ([Crockett et al. 2014](#)), Orion S ([Tahani et al. 2016](#); [Tahani 2013](#)), the Orion Bar ([Nagy et al. 2016](#)), and Sgr B2(N) ([Neill et al. 2014](#)).

Unlike the full spectral scans made of Sgr B2 and Orion sources, HIFI observations of W49N $[(\alpha, \delta) = (19^{\text{h}}10^{\text{m}}13^{\text{s}}.2, 09^{\circ}06'12.0'')]$ were made in targeted spectral windows as part of multiple science and calibration programs. In total, 5 CO transitions in the HIFI frequency range were observed toward W49N. CO $J = 6-5$ was covered by the PRISMAS (PRobing InterStellar Molecules with Absorption line Studies; KPGT_mgerin_1) key program in observations targeting D_2H^+ at 692 GHz, $J = 7-6$ by OT1_mgerin_4 in observations targeting C I at 809 GHz, and $J = 8-7$ by OT1_cvastel_2

¹ The $J = 12-11$ transition falls in the gap in frequency coverage.

in observations targeting HDO at 919 GHz. Observations of these three transitions utilized the WBS, and were made in DBS mode. On the fly (OTF) maps of CO $J = 10-9$ and $J = 13-12$ were made as part of calibration observations. Table 1 lists the ObsIDs that contain CO transitions for each source.

Sgr B2, Orion KL, the Orion Bar, and Orion S were also observed as part of the HEXOS program with the PACS spectrometer over the $\sim 54-190 \mu\text{m}$ spectral range, covering the $14 \leq J_u \leq 48$ rotational transitions of CO.² PACS observations of the Orion Bar will be presented by C. Joblin et al., (in preparation), so we do not discuss them further. The PRISMAS key program included PACS observations of W49N. The PACS spectrometer (Poglitsch et al. 2010) provides 25 spectra over a $47'' \times 47''$ field of view resolved in 5×5 spatial pixels (“spaxels”), each with an angular size of $9''.4 \times 9''.4$ on the sky. The resolving power of the grating spectrometer varies between $R \sim 1000-1500$ ($\sim 108-190 \mu\text{m}$ range), $R \sim 1700-3000$ ($70-94 \mu\text{m}$ range) and $R \sim 2700-5500$ ($54-70 \mu\text{m}$ range). Spectra for all sources were obtained in the pointed Range Spectroscopy SED mode. Orion S and W49N were observed in the standard “chop-nod” mode with a chopper throw of ± 6 arcmin. Owing to the very high far infrared continuum fluxes toward Sgr B2(M) and Orion KL (above the nominal saturation limits of PACS), these sources were observed in a specific non-standard engineering procedure (*PacsCalWaveCalNo-ChopBurst*; see Goicoechea et al. 2015). In order to avoid contamination from the bright Orion and Sgr B2 extended clouds, the “unchopped” observing mode was used. In this mode, background subtraction is achieved by removing the telescope spectrum measured on a distant reference OFF-position (in our case separated by ~ 20 arcmin). ObsIDs corresponding to these data are also shown in Table 1. Herein, we focus our analysis solely on the CO rotational transitions within the PACS and HIFI spectral scans.

3. DATA REDUCTION

3.1. HIFI

As mentioned in Section 2, HIFI observations of CO in W49N are comprised of data from multiple programs, such that our data set is not uniform. Single pointing observations of the $J = 6-5$ and $J = 7-6$ transitions were processed to Level 2 using the standard HIPE (*Herschel* Interactive Processing Environment; Ott 2010) pipeline v12.0, and those of the $J = 8-7$ transition were processed to Level 2 using HIPE v13.0. Baselines were subtracted using a first order polynomial and spectra taken at different LO frequencies were averaged together. Despite the beams for the H and V polarizations being separated by a few arcseconds, we found no evidence for sharp discrepancies between their associated spectra, so the two polarizations are also averaged together. OTF maps of the $J = 10-9$ and $J = 13-12$ transitions were processed to Level 2 via the standard HIPE pipeline v14.0 and converted to CLASS format. No spectrum in the OTF maps was taken at the same position as the single pointing observations. To extract a single spectrum at this position we take a weighted average of the spectra within the OTF maps. Individual spectra are weighted by $\exp(-r^2/\theta^2)$, where r is the angular separation between each observation and the single pointing position and θ is the radius of the HIFI beam (i.e., gaussian half width at half maximum) at the transition frequency.

The full HIFI spectral scans of Orion and Sgr B2 sources were processed using the same methods described in Neill et al. (2014). Orion S was processed through HIPE v9.0 (Tahani 2013), Orion KL through HIPE v10.3, and Sgr B2(M) through HIPE v8.0. These reduced data products are available for download via the *Herschel* Science Archive as user provided data products.³ All spectra were rescaled to account for the updated main beam efficiencies reported in Mueller et al. (2014).⁴ Resulting CO emission lines are shown in Figure 1.

3.2. PACS

PACS data were also processed using HIPE. Pointed observations with the PACS array do not provide fully spatially sampled maps. In particular, the individual spaxels do not fill the spectrometer point spread function (PSF) entirely. The measured width of the PSF is relatively constant for $\lambda \lesssim 100 \mu\text{m}$ (about the spaxel angular size) but increases at longer wavelengths. About 74% (41%) of the emission from a point source would fall in a given spaxel at about $54 \mu\text{m}$ ($190 \mu\text{m}$). For sources with semi-extended emission this means that accurate line fluxes can only be extracted by adding the fluxes measured in apertures that cover several spaxels. Orion KL and Sgr B2 data were calibrated and reduced as described in Goicoechea et al. (2015). Reductions of Orion S and W49N observations follow a similar method to that described in Gerin et al. (2015).

4. ANALYSIS

² Some wavelength ranges were affected by low spectral response ($98-102 \mu\text{m}$) and spectral leakage (see the PACS observer’s manual at http://herschel.esac.esa.int/Docs/PACS/html/pacs_om.html). We do not consider CO lines lying in these ranges.

³ <http://www.cosmos.esa.int/web/herschel/user-provided-data-products>

⁴ The HIFI Beam: Release #1; http://herschel.esac.esa.int/twiki/pub/Public/HifiCalibrationWeb/HifiBeamReleaseNote_Sep2014.pdf Table 2 and Equation 8, therein.

4.1. PACS Data

After data reduction and line identification, a polynomial baseline was subtracted in a narrow wavelength window around each detected CO line (with $J_u \geq 14$). Line fluxes (in W m^{-2}) were extracted by fitting Gaussians to every line detected in every spaxel. Total line fluxes (within a given aperture) were obtained by summing the line fluxes measured in the different individual spaxels. In most cases we added the fluxes from all 25 spaxels within the 5×5 PACS array. However, fluxes in Orion KL were determined as described in [Goicoechea et al. \(2015\)](#) for a 3×3 spaxel ($\approx 30'' \times 30''$) aperture centered on the hot core. This smaller region was used for extracting fluxes instead of the full array since the PACS footprint centered on Orion KL is contaminated by Orion H₂ Peak 1, which gives rise to most of the high- J CO emission (see Figure 1 in [Goicoechea et al. 2015](#)). The line fluxes towards Sgr B2(M) and Orion S were extracted from the full 5×5 spaxel aperture. In W49N we extracted CO line fluxes both from the central spaxel alone with a point source correction applied, and from the full 5×5 array. Our reasons for testing both methods are discussed in Section 4.3. The PACS flux calibration accuracy is limited by detector response drifts and slight pointing offsets, and the absolute flux calibration accuracy is estimated to be on the order of 30%.⁵ CO line fluxes determined from our analysis are reported in Table 2.

4.2. HIFI Data

Our analysis of the CO $5 \leq J_u \leq 16$ emission lines is performed using the spectra generated from the reduction described in Section 3.1. Integrated line fluxes ($\int T_{MB} dv$) in units of K km s^{-1} are extracted from the spectra in Figure 1 as described below, and are converted to intensity and flux via

$$\frac{\text{Intensity}}{(\text{W m}^{-2} \text{ sr}^{-1})} = \frac{\nu^3 2k_b}{c^3} \int T_{MB} dv = 1.0248 \times 10^{-18} \left(\frac{\nu}{\text{GHz}} \right)^3 \left(\frac{\int T_{MB} dv}{\text{K km s}^{-1}} \right) \quad (1)$$

and

$$\frac{\text{Flux}}{(\text{W m}^{-2})} = \frac{\nu^3 2k_b \Omega}{c^3} \int T_{MB} dv = 1.0248 \times 10^{-18} \left(\frac{\Omega}{\text{sr}} \right) \left(\frac{\nu}{\text{GHz}} \right)^3 \left(\frac{\int T_{MB} dv}{\text{K km s}^{-1}} \right) \quad (2)$$

where ν is the transition frequency, k_b is the Boltzmann constant, c is the speed of light, and Ω is the main beam solid angle. Line fluxes are reported in Table 2, along with Ω at the pertinent frequencies.

4.2.1. W49N

CO emission lines in W49N are shown in the top left panel of Figure 1. They display the same double peaked profiles as observed in HCN and HCO⁺ which are caused by strong self absorption and interpreted as a signature of gas infall ([Roberts et al. 2011](#)). The self absorption scenario is favored over two separate emission components because the weaker isotopologue emission (e.g., H¹³CO⁺, H¹³CN) is singly peaked at about 7 km s⁻¹, the systemic velocity of W49N. We determine integrated line fluxes for CO over the velocity interval from -40 to 45 km s⁻¹.

4.2.2. Orion KL

The top right panel of Figure 1 displays the CO emission lines observed toward Orion KL. The broad line profiles likely contain emission from the various well-known components such as the hot core, compact ridge, and plateau (high velocity and low velocity outflows), with the extended ridge giving rise to some of the self absorption near 10 km s⁻¹ ([Blake et al. 1987](#); [Crockett et al. 2014](#)). Integrated line fluxes were determined over the velocity interval from -80 to 90 km s⁻¹. Reported uncertainties account for the RMS noise level in the spectra (measured from -125 to -100 km s⁻¹) and the weak emission features caused by other species that are within the velocity interval over which we measure integrated fluxes. Note that all of the weak emission features seen in the Orion KL spectra at various LSR velocities are caused by molecules other than CO (e.g., SO₂ and CH₃OH). The emitting species have been identified and modeled by [Crockett et al. \(2014\)](#), and like the aforementioned reduced spectral scans, those models are also available as user provided data products.

4.2.3. Sgr B2(M)

Toward Sgr B2(M), CO emission is detected from all transitions covered by HIFI. Self-absorption caused by the Sgr B2 envelope is strong for transitions with $J_u \leq 8$, moderately strong for transitions with $9 \leq J_u \leq 11$, and either weak or not present for $J_u \geq 13$ transitions. Absorption due to gas in the foreground spiral arms is also seen for

⁵ PACS Spectroscopy performance and calibration, PACS/ICC document ID P1CC-KL-TN-041 (Vandenbussche et al.).

$J_u \leq 8$ transitions at velocities blue-shifted from 63 km s^{-1} , the systemic velocity of Sgr B2(M). All of these features are shown in the bottom left panel of Figure 1. These results parallel those found for Sgr B2(N) (Neill et al. 2014). CO line fluxes reported in Table 2 for Sgr B2(M) are integrated over the velocity range $0\text{--}130 \text{ km s}^{-1}$.

4.2.4. Orion S

Orion S is comprised of multiple physical components that can be distinguished via their differing kinematics. CO emission lines in Orion S are shown in the bottom right panel of Figure 1, and they display a narrow (FWHM $\approx 2 \text{ km s}^{-1}$) component centered at about 8.5 km s^{-1} , a medium (FWHM $\approx 7 \text{ km s}^{-1}$) component centered at about 7 km s^{-1} , and a broad (FWHM $\approx 20 \text{ km s}^{-1}$) component centered at about 5 km s^{-1} . This structure mimics that of H_2O emission observed toward both low and high mass protostars (e.g., Kristensen et al. 2012; San José-García et al. 2016). We fit these three components with gaussian functions, and our decomposition of the CO emission for select transitions is shown in left-hand side of Figure 2. The profile of the narrow component at 8.5 km s^{-1} is similar to that of CO emission in the Orion Bar (Nagy et al. 2013), and likely arises from the portion of Orion S that is being illuminated by the Trapezium stars, i.e., in a PDR. The medium component accounts for most of the line flux and is likely due to shocks associated with protostellar activity within the region. The broad component likely corresponds to the outflows detected in SiO (Ziurys et al. 1990) and CO (Schmid-Burgk et al. 1990). A fourth component is visible in Figure 3 as weak emission ($< 1 \text{ K}$) extending to high velocities ($\pm 80 \text{ km s}^{-1}$), and is detected for all transitions with $J_u \leq 11$. This emission corresponds to the highly collimated outflows observed in CO $J = 2\text{--}1$ by Zapata et al. (2005). It is not detected in the $J_u \geq 13$ transitions simply because the HIFI beam at these frequencies no longer encompasses any portion of the collimated outflows.

Careful inspection of the CO emission lines from Orion S in Figure 1 reveals that the $J = 5\text{--}4$, $6\text{--}5$, and $11\text{--}10$ profiles peak at velocities about 0.5 km s^{-1} lower than the other transitions, and show what appear as small absorption features at about 11 km s^{-1} . These artifacts are due to imperfect removal of CO emission that was in the reference beam at the off position (Tahani et al. 2016). As a result, the fit parameters for the different gaussian components (i.e., v_{LSR} , FWHM, and $\int T dv$) found for these transitions do not agree with those found for the unaffected transitions, and we exclude them from the remainder of our analysis. Using our fits to the CO emission lines we can generate SLEDs for each of the three different components as shown in the right-hand side of Figure 2. All three components show roughly the same overall shape, with SLEDs peaking around $J_u = 14$.

4.3. Combining PACS and HIFI Results

For Orion S, Orion KL, and Sgr B2(M) we have determined fluxes for the $J_u = 14$, 15 , and 16 transitions from both HIFI and PACS observations. As can be seen in Table 2, the values determined from the two different instruments do not agree. To generate a CO SLED without discontinuities, we scale HIFI fluxes given the following reasoning. In the limit of an unresolved point source, the flux measured is independent of the beam size. In the limit of a resolved source with uniform emission, the intensity measured is independent of beam size. By comparing PACS fluxes to HIFI fluxes and PACS intensities to HIFI intensities, we can determine which scenario is more likely applicable for each source. For Orion S, the PACS fluxes reported in Table 2 come from the full 5×5 spaxel array ($47 \times 47 \text{ arcsec}$). Fluxes for the $J_u = 14$, 15 , and 16 transitions determined from HIFI are lower than those determined from PACS, while intensities determined from HIFI are higher than those determined from PACS. For all three transitions, a roughly constant scaling factor (6% variation) can be used to convert PACS intensities to HIFI intensities, but not to convert PACS fluxes to HIFI fluxes ($\sim 50\%$ variation). This potentially indicates a source size that is larger than the HIFI beam(s), but smaller than the PACS 5×5 footprint, a scenario confirmed by inspection of the mid- J CO emission lines observed in each individual spaxel toward Orion S. If so, then the fluxes measured by PACS are correct, while those measured by HIFI are too low. Similarly, the intensities measured by HIFI are correct, while those measured by PACS are underestimated. Dividing the PACS flux by the HIFI intensity gives the source size (assuming uniform emission), and this can be used to scale the HIFI fluxes to the values that would have been measured had the beams fully encompassed the emitting region. In this way, we remove the discrepancies between the PACS and HIFI fluxes reported in Table 2, which would otherwise appear as discontinuities in the various CO SLEDs. The scaling factors used in this conversion for each source are: $2.58 \times 10^{-8}/\Omega$ for Orion S, $1.11 \times 10^{-8}/\Omega$ for Orion KL, and $9.21 \times 10^{-9}/\Omega$ for Sgr B2(M), where Ω is the beam solid angle at the transition frequency as reported in Table 2.

For W49N no CO transition was observed by both PACS and HIFI. Examination of CO spectra observed with each PACS spaxel reveals that the emitting region changes as a function of upper state energy. The lowest lines show emission over multiple spaxels, while the highest lines are concentrated in only the central spaxel. This is demonstrated in Figure 4 where the $J=14\text{--}13$ and $J = 28\text{--}27$ spectra in each PACS spaxel show differences in the

emitting region. Because of the changing source size, CO line fluxes extracted from the full 5×5 array are larger than those extracted from the central spaxel alone with a point source correction applied, except at high J_u where the emission becomes concentrated. The HIFI beams for the observed CO transitions are larger than 1 spaxel, smaller than the full PACS array, and also smaller than the CO emitting region seen in the HIFI OTF integrated intensity maps, further complicating the analysis. We choose to use the 5×5 PACS fluxes throughout the remainder of our analysis in order to avoid “throwing away” flux from the mid- J CO lines. HIFI fluxes are scaled by $1.23 \times 10^{-8}/\Omega$ to remove the discontinuity between PACS and HIFI fluxes. All of these issues highlight the difficulties inherent in combining emission line fluxes extracted from detectors with different beam sizes covering different portions of a target region that itself changes size and shape as a function of transition energy.

5. DISCUSSION

The CO SLEDs resulting from the analysis described above are shown in the top panel of Figure 5 for Sgr B2(M), Orion KL, Orion S, and W49N. Additionally, the top panel displays CO SLEDs in the Galactic sources Orion H₂ Peak 1 (Goicoechea et al. 2015), the Orion Bar (C. Joblin in preparation), and Sgr A* (Goicoechea et al. 2013), while the bottom panel shows CO SLEDs from the Seyfert 2 galaxy NGC 1068 (Spinoglio et al. 2012; Hailey-Dunsheath et al. 2012; Janssen et al. 2015), luminous infrared galaxies NGC 6240 (Mashian et al. 2015; Rosenberg et al. 2015) and NGC 4418 (Mashian et al. 2015; Rosenberg et al. 2015), and the starburst galaxy M 82 (Kamenetzky et al. 2012; Mashian et al. 2015). The vertical axes in both the top and bottom panels have been scaled to facilitate direct visual comparison of the CO SLED shapes. We focus first on the CO SLEDs in Galactic sources.

All of the Orion sources are at a distance of about 420 pc (Menten et al. 2007), so differences in those SLEDs are mostly intrinsic to the sources. The Orion Bar shows the simplest profile, and can be considered a template for the CO SLED in a strongly illuminated PDR with $\chi_{UV} \approx 10^4$ (expressed in units of the mean interstellar radiation field from Draine 1978). The other Orion sources likely contain PDR components as well, as some portion of the gas is being illuminated by FUV photons from the Trapezium cluster. Indeed, the decomposition of Orion S line profiles described in Section 4.2.4 shows this PDR component, and demonstrates that it has the smallest contribution to the total emission line flux. Orion S and Orion KL are both regions of embedded massive star formation, and the internal energy provided by this process through outflows, shocks, and radiation serves to increase the CO line flux compared to the externally heated Orion Bar. Orion KL has a bolometric luminosity about 10 times that of Orion S (O’Dell et al. 2008, and references therein), hence the larger CO line fluxes. Simply put, the increasing energy available going from the Orion Bar to Orion S to Orion KL both excites a larger amount of molecular gas and pushes population in the rotational levels of CO to higher J , thus producing the observed CO SLEDs. The SLED for Orion H₂ Peak 1—a region which can be considered a prototypical strong molecular shock—has a different shape with line fluxes decreasing more slowly as J_u increases. Excitation in this region is dominated by shock heating as a high-velocity outflow collides with quiescent molecular gas, and emission from the highest J_u transitions arises from hot ($T \sim 3000$ K), dense ($n \sim 10^7$ cm⁻³) gas (Goicoechea et al. 2015).

The Sgr B2(M) and Orion Bar SLEDs are very similar, despite the sources themselves and their CO emission line profiles being vastly different. As shown in Figure 1 the Sgr B2(M) line profiles are complex and dominated by self-absorption from the envelope that surrounds the hot core, whereas the Orion Bar has a single velocity component in emission (see, e.g., Figure 2 in Nagy et al. 2013). Additionally, far-infrared extinction by the Sgr B2 envelope may reduce the observed flux in the $J = 16$ –15 transition by a factor of 10 below that actually produced by Sgr B2(M) (Etxaluze et al. 2013), and by even larger factors for higher J_u lines (hence the non-detections for $J_u > 16$ transitions). While far IR extinction only affects certain objects, it is clear that attempting to infer source attributes from the CO line fluxes alone is a complicated and likely degenerate procedure.

The CO SLED in W49N most closely resembles that in Orion S. W49N is one of the most luminous massive star forming regions in our Galaxy—about 10^3 times more luminous than Orion S (Sievers et al. 1991)—and has been considered a template for extragalactic giant H II regions (Wu et al. 2016), so this similarity is unexpected. Nagy et al. (2012) concluded that both UV photons and mechanical processes (e.g., winds and outflows) are likely the dominant heating mechanisms in this region, while X-rays do not contribute significantly. It seems likely then that Orion S experiences similar conditions, just on a much smaller scale. Of the Galactic sources shown in Figure 5, the CO SLED in Sgr A* peaks at the lowest value of J_u . Goicoechea et al. (2013) concluded that UV photons and shocks are responsible for heating the hot molecular gas giving rise to the CO emission near Sgr A*, and that presently neither X-rays nor cosmic rays play a large role.

A multitude of galaxies have been observed by *Herschel* with SPIRE (e.g., Kamenetzky et al. 2014; Rosenberg et al. 2015) and PACS (e.g., Mashian et al. 2015) with CO emission lines as a primary target. We selected the 4 galaxies

shown in the bottom panel of Figure 5 for comparison to our Galactic sources because they present a variety of CO SLED shapes, including a member of each of the three classes defined by Rosenberg et al. (2015). Additionally, NGC 1068 and NGC 6240 have CO emission detected out to the highest J_u of any galaxies, providing the most extensive comparisons to Galactic regions, and the CO SLED of NGC 4418 peaks at the highest J_u of any galaxy. Note that we have excluded the SPIRE observations of NGC 1068 for $4 \leq J_u \leq 8$ as the larger beam at these frequencies contains two emission regions—circumnuclear disk (CND) and extended ring—whereas the SPIRE $J_u \geq 9$ and PACS $J_u \geq 14$ observations only probe the nuclear disk (Spinoglio et al. 2012; Hailey-Dunsheath et al. 2012).

It is immediately apparent that the extragalactic CO SLEDs differ in shape from their Galactic counterparts. In fact, linear combinations of the Orion, W49N, and Sgr B2(M) CO SLEDs are incapable of reproducing those seen in M 82, NGC 1068, and NGC 6240 because all of these Galactic SLEDs peak at higher J_u than the extragalactic SLEDs. Even the individual components of Orion S shown in Figure 2 fail in this regard. Only the Sgr A* CO SLED peaks at low enough J_u that it could conceivably be used to re-construct the extragalactic sources, while only the NGC 4418 CO SLED peaks at high enough J_u that it could conceivably be reproduced by Galactic sources. These disparities effectively prevent the empirical interpretation of extragalactic CO SLEDs and their underlying excitation mechanisms, yet simultaneously beg the question: Why do most Galactic CO SLEDs not resemble those in other galaxies?

The clearest difference between Galactic and extragalactic CO SLEDs is where the distribution peaks (i.e., which CO emission line has the largest flux). The NGC 4418 CO SLED peaks at $J_u \approx 11$ –13, the NGC 6240 and M 82 SLEDs at $J_u = 8$, while the NGC 1068 SLED is increasing toward lower J_u , with $J_u = 9$ being the lowest transition where the measured flux arises solely in the CND component. The Orion KL and Orion H₂ Peak 1 SLEDs peak near $J_u = 18$ with emission in Peak 1 extending all the way to $J_u = 48$, while the Orion Bar, Orion S, W49N, and Sgr B2(M) SLEDs peak near $J_u = 14$. Sgr A* has a CO SLED that peaks at $J_u = 8$. Where the CO SLEDs peak depends on the physical conditions of the gas, with hotter, denser gas leading to increased population, and thus flux, for higher J_u transitions. While it may at first seem counterintuitive that Galactic star forming regions appear to harbor more hot, dense molecular gas than regions surrounding active galactic nuclei (AGN), this is likely an effect of beam filling factors. At a distance of 14.4 Mpc (Bland-Hawthorn et al. 1997) the $9''.4 \times 9''.4$ central spaxel of PACS covers a region about 650 pc on a side in NGC 1068. For NGC 4418 at $d = 34$ Mpc (Braatz et al. 1997) and NGC 6240 at $d = 107$ Mpc (Meijerink et al. 2013) the central spaxel covers a region approximately 1.5×1.5 kpc and 4.6×4.6 kpc, respectively. CO line fluxes in M 82 were extracted from the full $47'' \times 47''$ PACS array (Mashian et al. 2015), which covers a region 770×770 pc at $d = 3.4$ Mpc (Dalcanton et al. 2009). These regions, which do contain hot, dense gas as evidenced by emission from high- J_u CO, must also contain large amounts of cooler gas which emit primarily at lower J_u transitions of CO. Emission from the hot, dense gas only fills a small portion of the beam, while emission from the more extended cooler gas fills a much larger portion of the beam and ends up dominating the CO SLED.

Beam filling effects have previously been invoked to describe CO SLEDs observed in the Galactic center. One scenario proposed by Goicoechea et al. (2013) to explain the Sgr A* CO SLED suggests that the hot gas responsible for the high- J_u emission is concentrated in small dense clumps that reside in a more diffuse, extended medium which gives rise to the lower J_u emission. Another study by Kamenetzky et al. (2014) compared the CO SLEDs of Sgr B2(M), Sgr B2(N), and the Sgr B2 envelope determined from SPIRE observations (Ettxaluze et al. 2013), to those of several other galaxies. They note that the CO SLED of the Sgr B2 envelope resembles those of other galaxies, while the CO SLEDs in the Sgr B2 cores (i.e., those specifically focused on hot gas) peak at higher J_u . Furthermore, Kamenetzky et al. (2014) conclude that while CO emission from star-forming cores must be present in their observations of other galaxies, the line flux is dominated by emission from warm, extended molecular clouds. In contrast, the observations of Galactic sources are tightly focused on known energetic regions. The full PACS footprint covers an area of about 0.1×0.1 pc in the Orion star-forming region ($d \approx 420$ pc), and about 2.5×2.5 pc in W49N ($d = 11.1 \pm 0.8$ kpc; Zhang et al. 2013). With hot, dense gas filling a large portion of the beam and a lack of “contamination” from unassociated cooler gas, the Galactic CO SLEDs peak at higher J_u .

6. SUMMARY

We have observed rotational transitions from the $5 \leq J_u \leq 16$ states of CO with HIFI and from $J_u \geq 14$ with PACS in emission toward Orion S, Orion KL, Sgr B2(M), and W49N. Fluxes are extracted from the CO emission lines and used to construct spectral line energy distributions (SLEDs). Our original intent was to empirically interpret CO SLEDs in other galaxies by reconstructing them from linear combinations of CO SLEDs in Galactic sources where the gas properties and heating mechanisms are well characterized. However, the CO SLEDs in our sample of Galactic sources all peak at higher J_u than the CO SLEDs observed in other galaxies, such that no combination can successfully

reproduce the extragalactic observations. The difference between Galactic and extragalactic CO SLEDs is primarily a beam filling effect. Our observations in the Milky Way specifically target star-forming cores, preferentially sampling hot molecular gas while excluding cold quiescent gas, such that the resulting CO SLEDs peak around $14 \lesssim J_u \lesssim 20$. In other galaxies the PACS and SPIRE beams cover much larger physical regions than they do within the Milky Way. As a result, in addition to the small pockets of hot, dense gas which produce high- J_u CO emission, these beams also sample a large amount of cooler, more extended gas. It is this material, filling a much larger portion of the beam than the hot dense gas, which dominates the CO emission and causes SLEDs to peak closer to $J_u \sim 8$. As such, we urge that careful consideration be given to these effects when comparing *Herschel* observations sampling vastly different physical size scales.

The authors thank the anonymous referee for suggestions to improve the clarity of the paper. Support for this work was provided by NASA through an award issued by JPL/Caltech. J.R.G. and J.C. thank the ERC for support under grant ERC-2013-Syg-610256-NANOCOSMOS, and the Spanish MINECO for support under grant AYA2012-32032. HIFI has been designed and built by a consortium of institutes and university departments from across Europe, Canada and the United States under the leadership of SRON Netherlands Institute for Space Research, Groningen, The Netherlands and with major contributions from Germany, France and the US. Consortium members are: Canada: CSA, U. Waterloo; France: CESR, LAB, LERMA, IRAM; Germany: KOSMA, MPIfR, MPS; Ireland, NUI Maynooth; Italy: ASI, IFSI-INAf, Osservatorio Astrofisico di Arcetri-INAf; Netherlands: SRON, TUD; Poland: CAMK, CBK; Spain: Observatorio Astronómico Nacional (IGN), Centro de Astrobiología (CSIC-INTA). Sweden: Chalmers University of Technology - MC2, RSS & GARD; Onsala Space Observatory; Swedish National Space Board, Stockholm University - Stockholm Observatory; Switzerland: ETH Zurich, FHNW; USA: Caltech, JPL, NHSC.

PACS has been developed by a consortium of institutes led by MPE (Germany) and including UVIE (Austria); KU Leuven, CSL, IMEC (Belgium); CEA, LAM (France); MPIA (Germany); INAF-IFSI/OAA/OAP/OAT, LENS, SISSA (Italy); IAC (Spain). This development has been supported by the funding agencies BMVIT (Austria), ESA-PRODEX (Belgium), CEA/CNES (France), DLR (Germany), ASI/INAF (Italy), and CICYT/MCYT (Spain).

REFERENCES

- Alves, J., & Homeier, N. 2003, *ApJL*, 589, L45
- Bergin, E. A., Phillips, T. G., Comito, C., et al. 2010, *A&A*, 521, L20
- Blake, G. A., Sutton, E. C., Masson, C. R., & Phillips, T. G. 1987, *ApJ*, 315, 621
- Bland-Hawthorn, J., Gallimore, J. F., Tacconi, L. J., et al. 1997, *Ap&SS*, 248, 9
- Braatz, J. A., Wilson, A. S., & Henkel, C. 1997, *ApJS*, 110, 321
- Crockett, N. R., Bergin, E. A., Neill, J. L., et al. 2014, *ApJ*, 787, 112
- Dalcanton, J. J., Williams, B. F., Seth, A. C., et al. 2009, *ApJS*, 183, 67
- de Graauw, T., Helmich, F. P., Phillips, T. G., et al. 2010, *A&A*, 518, L6
- Draine, B. T. 1978, *ApJS*, 36, 595
- Etxaluze, M., Goicoechea, J. R., Cernicharo, J., et al. 2013, *A&A*, 556, A137
- Galván-Madrid, R., Liu, H. B., Zhang, Z.-Y., et al. 2013, *ApJ*, 779, 121
- Gerin, M., Ruaud, M., Goicoechea, J. R., et al. 2015, *A&A*, 573, A30
- Goicoechea, J. R., Etxaluze, M., Cernicharo, J., et al. 2013, *ApJL*, 769, L13
- Goicoechea, J. R., Chavarría, L., Cernicharo, J., et al. 2015, *ApJ*, 799, 102
- Griffin, M. J., Abergel, A., Abreu, A., et al. 2010, *A&A*, 518, L3
- Hailey-Dunsheath, S., Sturm, E., Fischer, J., et al. 2012, *ApJ*, 755, 57
- Henney, W. J., O'Dell, C. R., Zapata, L. A., et al. 2007, *AJ*, 133, 2192
- Janssen, A. W., Bruderer, S., Sturm, E., et al. 2015, *ApJ*, 811, 74
- Kamenetzky, J., Rangwala, N., Glenn, J., Maloney, P. R., & Conley, A. 2014, *ApJ*, 795, 174
- Kamenetzky, J., Glenn, J., Rangwala, N., et al. 2012, *ApJ*, 753, 70
- Kristensen, L. E., van Dishoeck, E. F., Bergin, E. A., et al. 2012, *A&A*, 542, A8
- Mashian, N., Sturm, E., Sternberg, A., et al. 2015, *ApJ*, 802, 81
- Meijerink, R., Kristensen, L. E., Weiß, A., et al. 2013, *ApJL*, 762, L16
- Menten, K. M., Reid, M. J., Forbrich, J., & Brunthaler, A. 2007, *A&A*, 474, 515
- Murakami, H., Koyama, K., Sakano, M., Tsujimoto, M., & Maeda, Y. 2000, *ApJ*, 534, 283
- Nagy, Z., van der Tak, F. F. S., Fuller, G. A., Spaans, M., & Plume, R. 2012, *A&A*, 542, A6
- Nagy, Z., Van der Tak, F. F. S., Ossenkopf, V., et al. 2013, *A&A*, 550, A96
- Nagy, Z., Choi, Y., Ossenkopf-Okada, V., et al. 2016, *ArXiv e-prints*, arXiv:1611.07470
- Neill, J. L., Bergin, E. A., Lis, D. C., et al. 2014, *ApJ*, 789, 8
- Nissen, H. D., Cunningham, N. J., Gustafsson, M., et al. 2012, *A&A*, 540, A119
- O'Dell, C. R., Muench, A., Smith, N., & Zapata, L. 2008, *Star Formation in the Orion Nebula II: Gas, Dust, Proplyds and Outflows*, ed. B. Reipurth, 544
- Ott, S. 2010, in *Astronomical Society of the Pacific Conference Series*, Vol. 434, *Astronomical Data Analysis Software and Systems XIX*, ed. Y. Mizumoto, K.-I. Morita, & M. Ohishi, 139
- Peng, T.-C., Wyrowski, F., Zapata, L. A., Güsten, R., & Menten, K. M. 2012, *A&A*, 538, A12
- Pilbratt, G. L., Riedinger, J. R., Passvogel, T., et al. 2010, *A&A*, 518, L1

- Poglitsch, A., Waelkens, C., Geis, N., et al. 2010, *A&A*, 518, L2
- Rivilla, V. M., Martín-Pintado, J., Sanz-Forcada, J., Jiménez-Serra, I., & Rodríguez-Franco, A. 2013, *MNRAS*, 434, 2313
- Roberts, H., van der Tak, F. F. S., Fuller, G. A., Plume, R., & Bayet, E. 2011, *A&A*, 525, A107
- Rosenberg, M. J. F., van der Werf, P. P., Aalto, S., et al. 2015, *ApJ*, 801, 72
- San José-García, I., Mottram, J. C., van Dishoeck, E. F., et al. 2016, *A&A*, 585, A103
- Schmid-Burgk, J., Guesten, R., Mauersberger, R., Schulz, A., & Wilson, T. L. 1990, *ApJL*, 362, L25
- Sievers, A. W., Mezger, P. G., Bordeon, M. A., et al. 1991, *A&A*, 251, 231
- Spinoglio, L., Pereira-Santaella, M., Busquet, G., et al. 2012, *ApJ*, 758, 108
- Tahani, K. 2013, Master's thesis, University of Calgary, Canada
- Tahani, K., Plume, R., Bergin, E. A., et al. 2016, *ApJ*, 832, 12
- van der Wiel, M. H. D., van der Tak, F. F. S., Ossenkopf, V., et al. 2009, *A&A*, 498, 161
- Wu, S.-W., Bik, A., Bestenlehner, J. M., et al. 2016, *A&A*, 589, A16
- Zapata, L. A., Ho, P. T. P., Rodríguez, L. F., et al. 2006, *ApJ*, 653, 398
- Zapata, L. A., Rodríguez, L. F., Ho, P. T. P., et al. 2005, *ApJL*, 630, L85
- Zapata, L. A., Schmid-Burgk, J., Ho, P. T. P., Rodríguez, L. F., & Menten, K. M. 2009, *ApJL*, 704, L45
- Zapata, L. A., Schmid-Burgk, J., & Menten, K. M. 2011, *A&A*, 529, A24
- Zhang, B., Reid, M. J., Menten, K. M., et al. 2013, *ApJ*, 775, 79
- Ziurys, L. M., Wilson, T. L., & Mauersberger, R. 1990, *ApJL*, 356, L25

Table 1. Observation Identifiers (ObsIDs) for Spectra Containing CO Emission

	Orion S	Orion KL	Sgr B2(M)	W49N
HIFI				
CO $J = 5-4$	1342204001	1342191592	1342191565	
CO $J = 6-5$	04708	194540	192546	1342194554, 5, 6
CO $J = 7-6$	05332	205334	204723	1342230253, 4, 5
CO $J = 8-7$	05336	192329	206455	1342244816, 7, 8
CO $J = 9-8$	03150	191601	218200	
CO $J = 10-9$	05871	191725	204739	1342253940, 68481
CO $J = 11-10$	16384	216387	215935	
CO $J = 13-12$	03925	1342191727, 8	192656	1342254900, 68195
CO $J = 14-13$	03948	1342191562, 3	206501	
CO $J = 15-14$	05534	1342194732, 3	216702	
CO $J = 16-15$	05540	1342192673, 4	206640	
PACS				
CO $J = 14-13$ through 35-34	1342218570	1342218575	1342206883	1342207774
CO $J = 36-35$ through 48-47	1342218569	1342218576		1342207775

Table 2. CO Line Fluxes

Transition	Orion S		Orion KL		Sgr B2(M)		W49N	
	Ω (10^{-9} sr)	(10^{-15} W m $^{-2}$)	(10^{-15} W m $^{-2}$)	Flux (10^{-15} W m $^{-2}$)	(10^{-15} W m $^{-2}$)	(10^{-15} W m $^{-2}$)	(10^{-15} W m $^{-2}$)	(10^{-15} W m $^{-2}$)
HIFI								
$J = 5-4$	24.0	3.53 \pm 0.05	26.2 \pm 0.3	1.37 \pm 0.03
$J = 6-5$	17.1	4.59 \pm 0.06	37.5 \pm 0.4	2.54 \pm 0.01	4.80 \pm 0.24
$J = 7-6$	12.3	5.61 \pm 0.04	41.8 \pm 0.5	5.16 \pm 0.02	5.16 \pm 0.26
$J = 8-7$	9.44	6.17 \pm 0.04	51.5 \pm 0.5	6.05 \pm 0.16	5.86 \pm 0.29
$J = 9-8$	7.52	6.37 \pm 0.05	57.9 \pm 0.6	7.74 \pm 0.11
$J = 10-9$	6.64	7.12 \pm 0.04	66.1 \pm 0.7	8.08 \pm 0.21	6.79 \pm 0.34
$J = 11-10$	5.49	6.51 \pm 0.05	74.3 \pm 0.8	7.23 \pm 0.16
$J = 12-11$
$J = 13-12$	3.59	5.94 \pm 0.09	67.9 \pm 0.9	4.82 \pm 0.14	5.43 \pm 0.27
$J = 14-13$	3.09	5.25 \pm 0.07	66.1 \pm 1.0	5.11 \pm 0.29
$J = 15-14$	2.78	4.25 \pm 0.08	65.4 \pm 1.1	5.25 \pm 0.10
$J = 16-15$	2.45	2.97 \pm 0.07	61.2 \pm 1.1	3.24 \pm 0.14
PACS		5 \times 5	3 \times 3	5 \times 5	5 \times 5
$J = 14-13$		41.58	230.3	18.00	17.60
$J = 15-14$		37.93	253.9	15.28	18.30
$J = 16-15$		33.89	294.2	11.41	16.00
$J = 17-16$		27.78	323.0	...	13.90
$J = 18-17$		21.91	269.0	...	11.10
$J = 19-18$		15.34	318.4	...	12.60
$J = 20-19$		12.65	317.5	...	11.50
$J = 21-20$		9.23	263.4	...	9.23
$J = 22-21$		5.65	233.9	...	7.73
$J = 23-22$		14.97	5.76
$J = 24-23$		3.99	156.4	...	4.95
$J = 25-24$		3.70	3.26
$J = 26-25$	
$J = 27-26$		2.20
$J = 28-27$		2.74	56.5	...	2.22
$J = 29-28$		2.04	32.9	...	1.91
$J = 30-29$		1.90	32.9	...	1.14
$J = 31-30$	
$J = 32-31$...	22.2	...	0.86
$J = 33-32$...	20.1	...	0.36
$J = 34-33$...	12.7	...	0.34
$J = 35-34$...	7.0
$J = 36-35$...	5.0
$J = 37-36$...	3.1
$J = 38-37$...	4.2
$J = 39-38$...	2.2
$J = 40-39$...	1.3
$J = 41-40$...	0.9
$J = 42-41$...	0.8

NOTE—Absolute flux calibration accuracy is estimated to be about 30% for PACS.

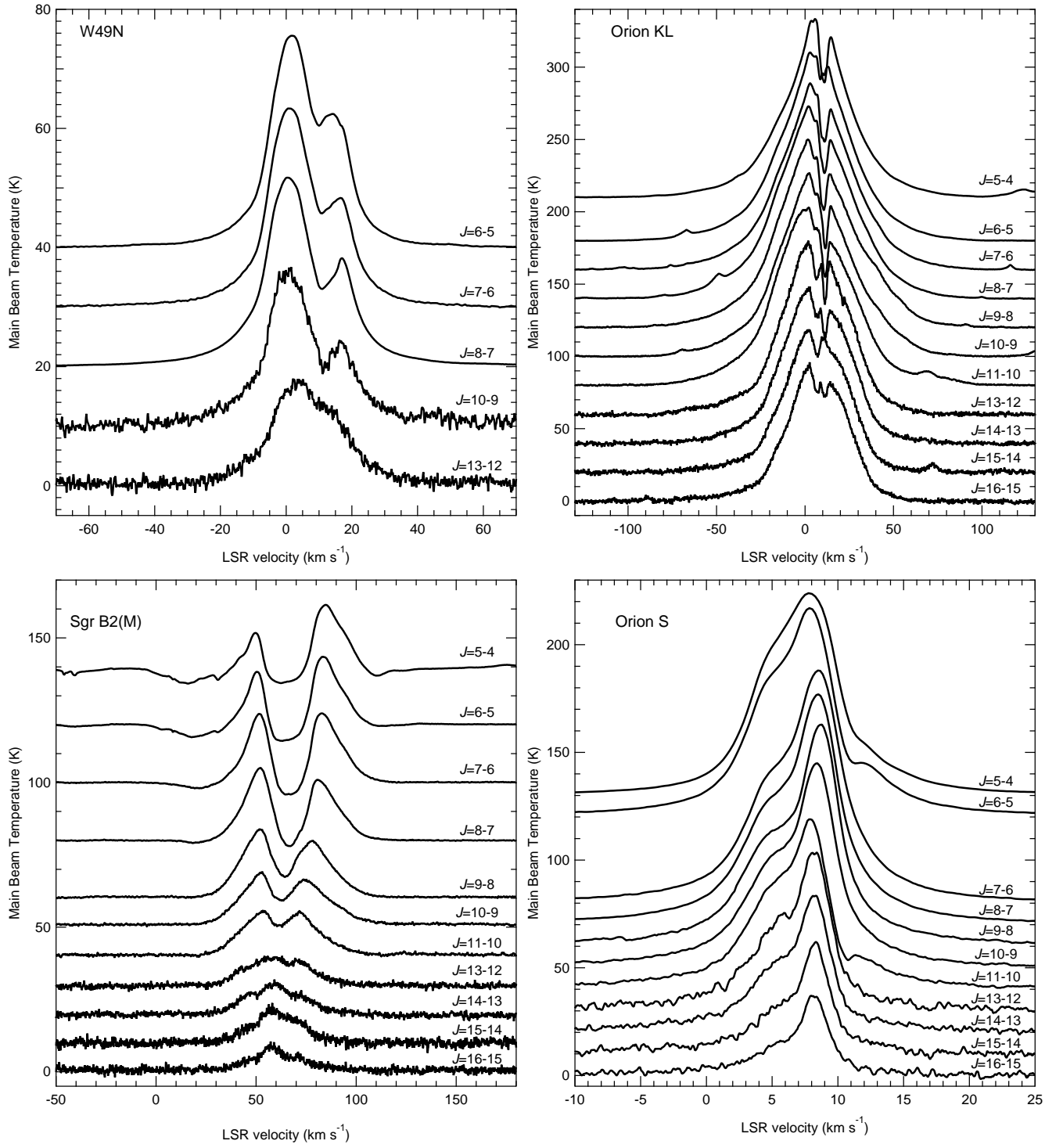


Figure 1. CO emission lines in W49N (top left), Orion KL (top right), Sgr B2(M) (bottom left) and Orion S (bottom right). Note the different velocity and temperature scales in each panel. Spectra are shifted vertically for clarity. In Orion KL the spectra displayed for the $13 \leq J_u \leq 16$ transitions are from the observations targeting the compact ridge.

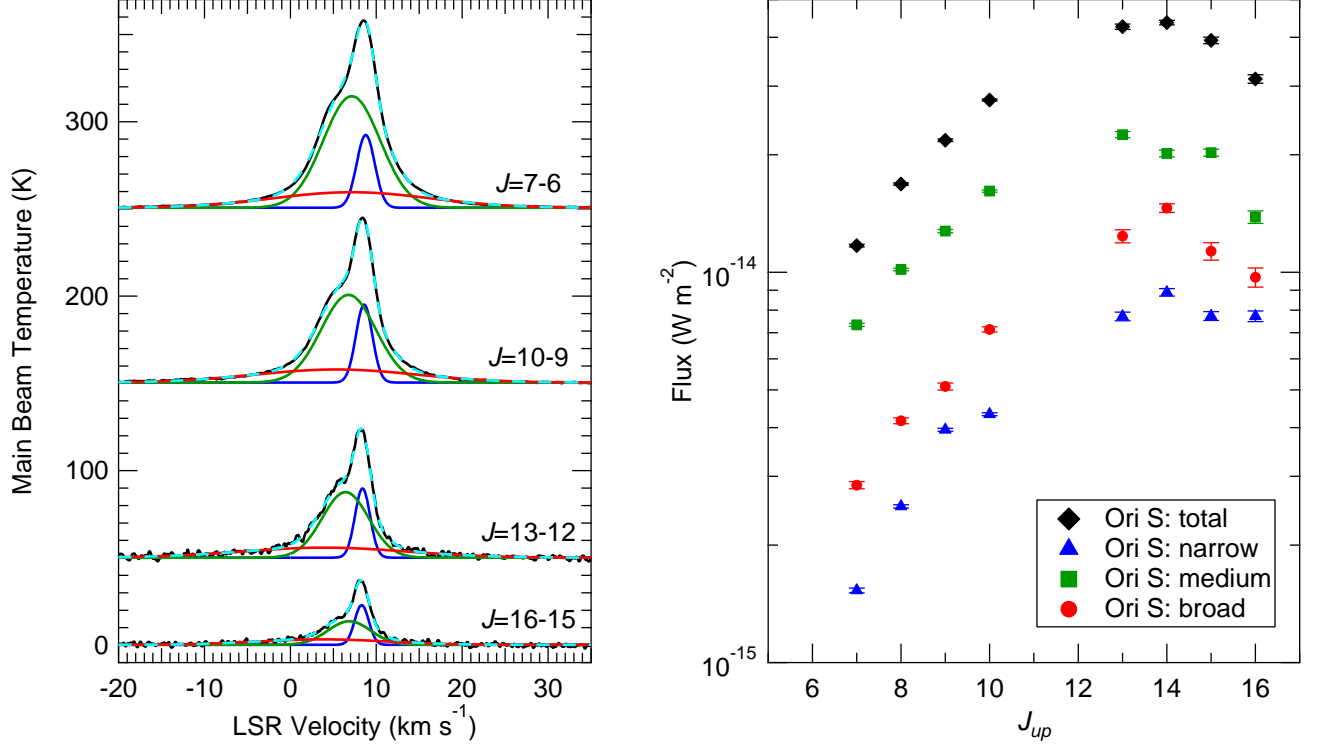


Figure 2. The decomposition of select CO transitions toward Orion S into three gaussian components is displayed on the left. Spectra are shown in black, with the full fit given by dashed cyan curves. The narrow PDR component is shown in blue, the shock component in green, and the broad outflow component in red. Fluxes for each of the components—scaled as described in Section 4.3—are plotted on the right side. Color coding matches the fit components in the left panel, although the total flux is marked by black (rather than cyan) diamonds. Flux uncertainties are generally smaller than the plotted markers.

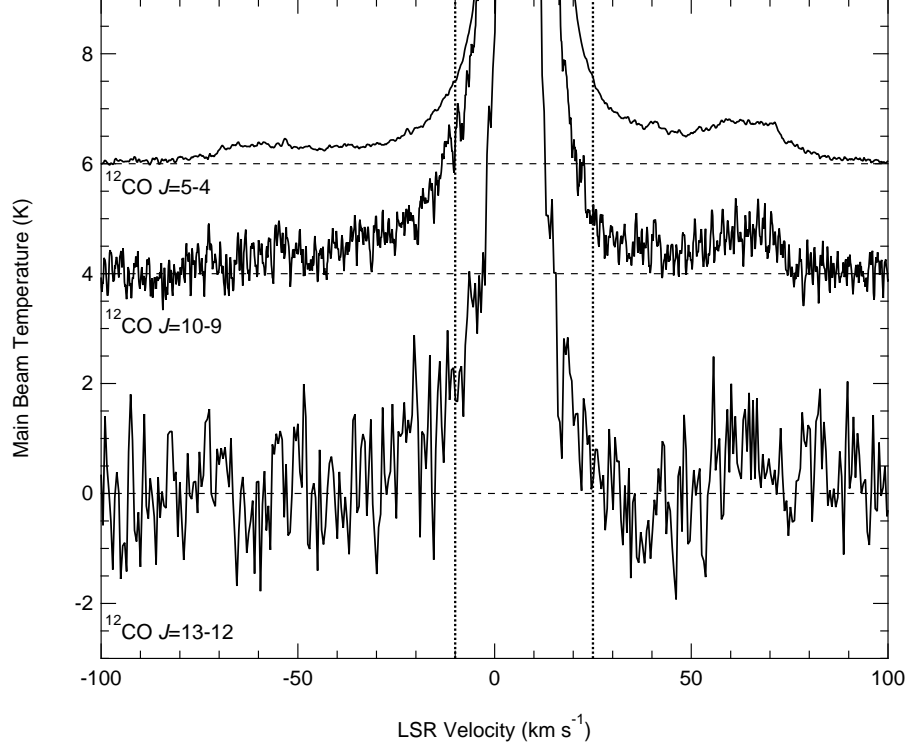


Figure 3. Zoom in on select CO transitions toward Ori S showing CO “bullets”. Spectra have been shifted vertically for clarity, and the zero level for each spectrum is marked by a horizontal dashed line. The $J = 13-12$ spectrum has been smoothed to 0.5 km s^{-1} resolution. Vertical dotted lines denote the full velocity range shown in the bottom right panel of Figure 1.

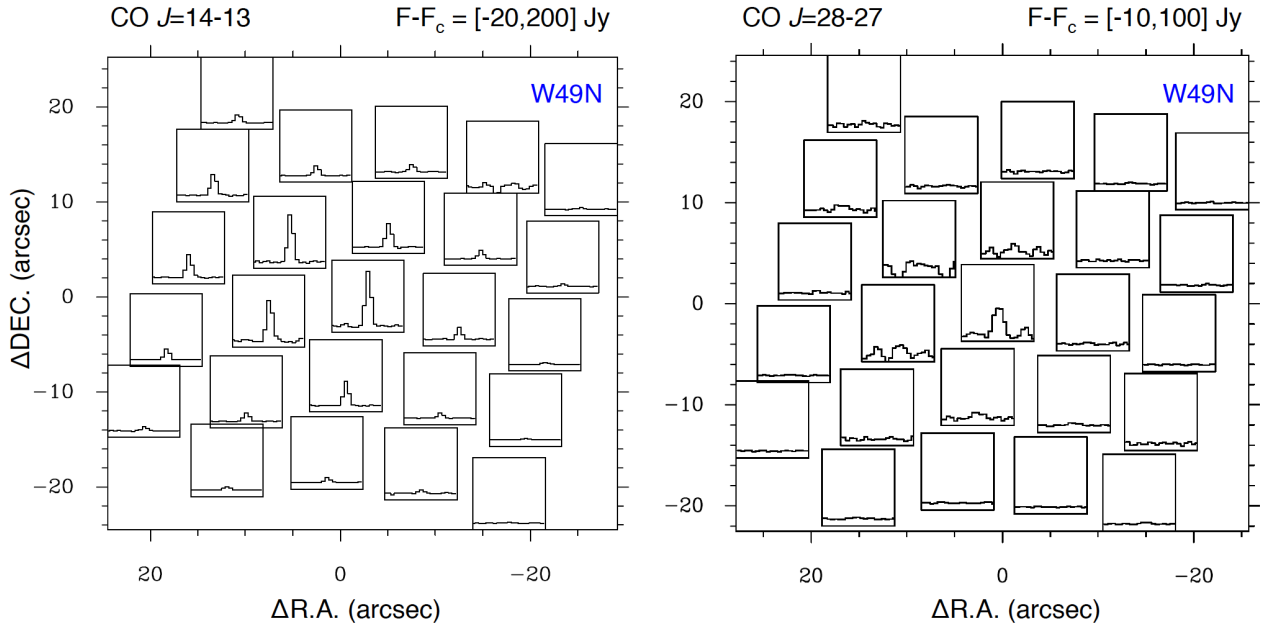


Figure 4. Continuum-subtracted high- J CO maps for W49N obtained with the PACS array in 25 spaxels. The line flux scale (in Jy) is indicated in the top-right of each panel. The $(0,0)$ position corresponds to $(\alpha, \delta) = (19^{\text{h}}10^{\text{m}}13^{\text{s}}.1, 09^{\circ}06'12.0'')$.

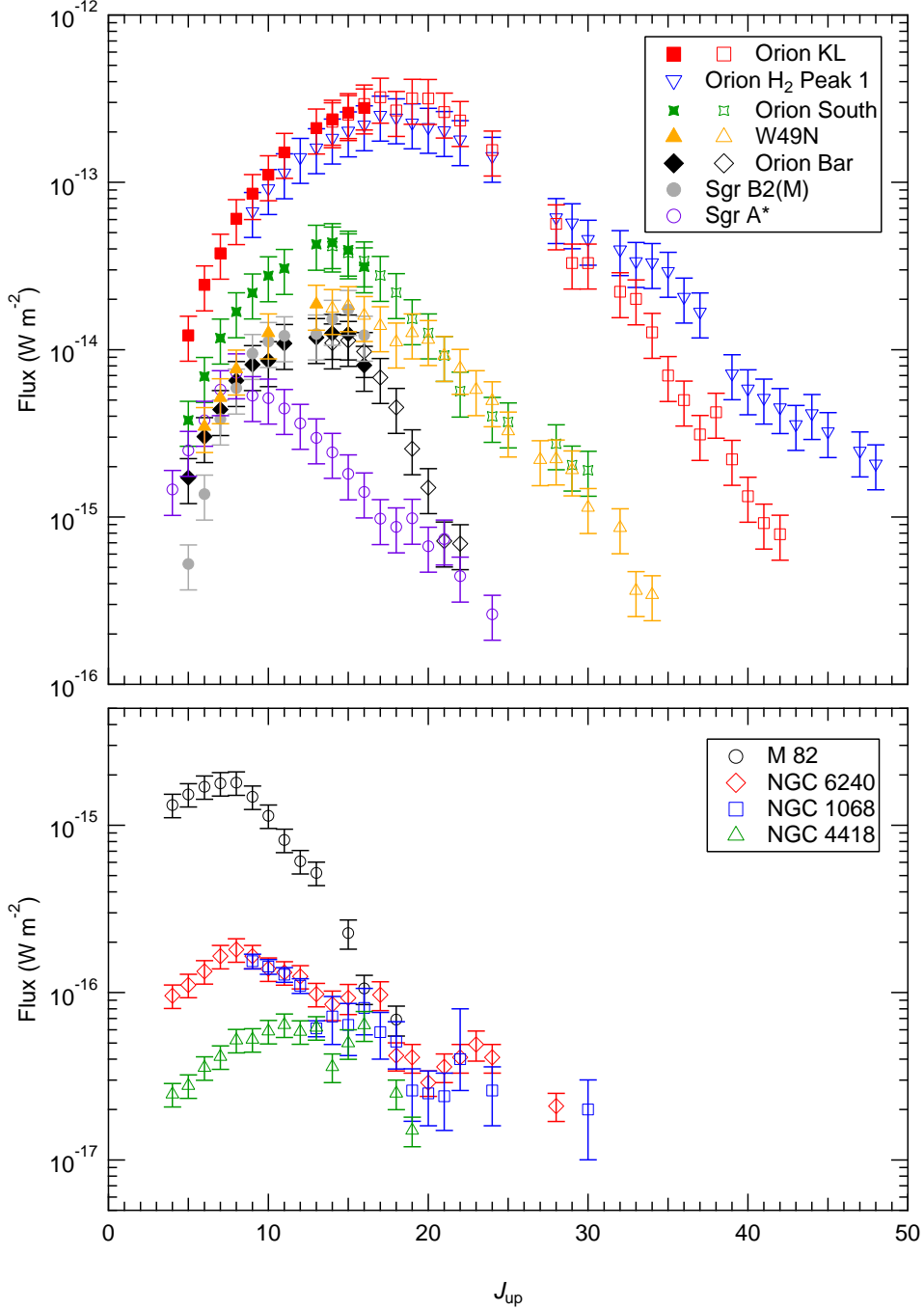


Figure 5. CO spectral line energy distributions for Galactic sources (top), and for extragalactic sources (bottom). Filled symbols denote fluxes determined from HIFI observations, and open symbols from either SPIRE ($J_u \leq 13$) or PACS ($J_u \geq 14$) observations. The 30% uncertainties in PACS fluxes have been applied to the HIFI fluxes as well given our scaling procedure. References for published line fluxes are as follows: Orion H₂ Peak 1 (Goicoechea et al. 2015); Orion Bar (C. Joblin in prep.); Sgr A* (Goicoechea et al. 2013); NGC 1068 (Spinoglio et al. 2012; Hailey-Dunsheath et al. 2012; Janssen et al. 2015); NGC 6240 (Rosenberg et al. 2015; Mashian et al. 2015); M 82 (Kamenetzky et al. 2012; Mashian et al. 2015); NGC 4418 (Rosenberg et al. 2015; Mashian et al. 2015).